Targeted polyelectrolyte complex micelles treat vascular complications in vivo

Zhengjie Zhou[a,b], Chih-Fan Yeh[b,c], Michael Mellas[a], Myung-Jin Oh[b], Jiayu Zhu[b], Jin Li[b], Ru-Ting Huang[b], Devin L. Harrison[b,d], Tzu-Pin Shentu[b], David Wu[b], Michael Lueckheide[a], Lauryn Carver[a,b], Eun Ji Chung[a], Lorraine Leon[a], Kai-Chien Yang[c], Matthew V. Tirrell[a,d,e,1], and Yun Fang[b,d,1]

[a]Pritzker School of Molecular Engineering, University of Chicago, Chicago, IL 60637; [b]Biological Sciences Division, Department of Medicine, University of Chicago, Chicago, IL 60637; [c]Division of Cardiology, Department of Internal Medicine and Cardiovascular Center, National Taiwan University Hospital, Taipei 100, Taiwan; [d]Graduate Program in Biophysical Sciences, University of Chicago, Chicago, IL 60637; and [e]Materials Science Division, Argonne National Laboratory, Lemont, IL 60439

This contribution is part of the special series of Inaugural Articles by members of the National Academy of Sciences elected in 2019.

Contributed by Matthew V. Tirrell; received August 12, 2021; accepted November 1, 2021; reviewed by Shu Chien and Erkki Ruoslahti

Vascular disease is a leading cause of morbidity and mortality in the United States and globally. Pathological vascular remodeling, such as atherosclerosis and stenosis, largely develop at arterial sites of curvature, branching, and bifurcation, where disturbed blood flow activates vascular endothelium. Current pharmacological treatments of vascular complications principally target systemic risk factors. Improvements are needed. We previously devised a targeted polyelectrolyte complex micelle to deliver therapeutic nucleotides to inflamed endothelium in vitro by displaying the peptide VHPKQHR targeting vascular cell adhesion molecule 1 (VCAM-1) on the periphery of the micelle. This paper explores whether this targeted nanomedicine strategy effectively treats vascular complications in vivo. Disturbed flow-induced microRNA-92a (miR-92a) has been linked to endothelial dysfunction. We have engineered a transgenic line (*miR-92a*$^{EC\text{-}TG}$/*Apoe*$^{-/-}$) establishing that selective miR-92a overexpression in adult vascular endothelium causally promotes atherosclerosis in *Apoe*$^{-/-}$ mice. We tested the therapeutic effectiveness of the VCAM-1–targeting polyelectrolyte complex micelles to deliver miR-92a inhibitors and treat pathological vascular remodeling in vivo. VCAM-1–targeting micelles preferentially delivered miRNA inhibitors to inflamed endothelial cells in vitro and in vivo. The therapeutic effectiveness of anti–miR-92a therapy in treating atherosclerosis and stenosis in *Apoe*$^{-/-}$ mice is markedly enhanced by the VCAM-1–targeting polyelectrolyte complex micelles. These results demonstrate a proof of concept to devise polyelectrolyte complex micelle-based targeted nanomedicine approaches treating vascular complications in vivo.

nanoparticle | nanomedicine | atherosclerosis | vascular remodeling | stenosis

Dysfunction of vasculature contributes enormously to human diseases but vascular wall-targeted therapies are challenging to develop and scant. Current pharmacological treatments for vascular complications mainly address systematic risk factors but do not target the diseased blood vessel per se. Treatments of vascular disease remain suboptimal. Atherosclerosis, thickening and hardening of arterial walls, is a leading cause of mortality and morbidity in the United States and worldwide (1). Despite well-established systemic risk factors, such as hypercholesterolemia and hypertension, atherosclerosis and pathological vascular remodeling largely occur in vascular sites, such as curvatures, bifurcations, and bifurcations where local disturbed blood flow activates vascular endothelial cells (2–6). In contrast, the straight parts of the artery are exposed to unidirectional flow and are largely resistant to atherosclerosis. This observation highlights a unique opportunity. There is tremendous potential to devise innovative therapeutic strategies targeting activated endothelium to treat atherosclerosis and vascular complications.

Predominant roles of microRNA (miRNA) in mediating human diseases, including vascular complications, have been increasingly uncovered in recent years (6–8). Dysregulated miRNAs are attractive therapeutic candidates since a single miRNA typically targets multiple genes that are often within the same pathway (9, 10). Nevertheless, it remains extremely challenging to deliver therapeutic nucleotides targeting dysregulated miRNAs to diseased tissues of interest (7). Systemic administration of nucleotides has typically resulted in unfavorable pharmacokinetic parameters, resulting from rapid in vivo degradation and poor cellular uptake, leading to low bioavailability in target cells and unwanted side effects in nontarget tissues (7). Studies by us and others have linked aberrant miRNA expression to key cellular events related to atherosclerosis (9–14). Specifically, disturbed flow markedly induces miR-92a in endothelial cells to increase vascular inflammation (10, 12–15). In addition, reduced atherosclerosis was reported in mice administered a naked form of miR-92a inhibitors in the circulation (13, 14); however, systemic delivery of miR-92a

Significance

Vascular disease is a leading cause of human morbidity and mortality and current therapies mainly target systemic risk factors but not the diseased vasculature per se. We have devised a targeted nanomedicine approach engineering self-assembled polyelectrolyte complex micelles that target inflamed vascular endothelium and simultaneously encapsulate therapeutic nucleic acids. We showed that this targeted nanomedicine strategy effectively delivers therapeutic nucleotides to inflamed endothelium in vivo. The causal role of increased endothelial miR-92a in driving atherosclerosis is established by a new transgenic mouse line. We demonstrated that targeted polyelectrolyte complex micelles significantly enhance the anti–miR-92a therapy treating vascular complications in vivo.

Author contributions: M.V.T. and Y.F. designed research; Z.Z., C.-F.Y., M.M., and M.-J.O. performed research; Z.Z., J.Z., J.L., R.-T.H., D.L.H., T.-P.S., D.W., and M.L. contributed new reagents/analytic tools; Z.Z., L.C., E.J.C., L.L., K.-C.Y., M.V.T., and Y.F. analyzed data; and Z.Z., M.V.T., and Y.F. wrote the paper.

Reviewers: S.C., University of California San Diego; and E.R., Sanford Burnham Prebys Medical Discovery Institute.

The authors declare no competing interest.

[1]To whom correspondence may be addressed. Email: mtirrell@uchicago.edu or yfang1@medicine.bsd.uchicago.edu.

This article contains supporting information online at http://www.pnas.org/lookup/suppl/doi:10.1073/pnas.2114842118/-/DCSupplemental.

Published December 8, 2021.

inhibitors was shown to result in miR-92a inhibition in a wide range of tissues in addition to vascular endothelium (14). It remains to be determined whether increased endothelial miR-92a per se causatively drives atherosclerosis in vivo.

Nucleotide-based therapies could revolutionize future medical practice. For example, dysregulated miRNA can be corrected by specific mimics/inhibitors (7). Polyelectrolyte complex micelles have great potential as gene-delivery vehicles due to the ability to encapsulate negatively charged nucleic acids forming a core by neutralizing the charge, while simultaneously protecting the nucleic acids from nonspecific interactions and enzymatic degradation (16, 17). Moreover, we demonstrated that polyelectrolyte complex micelles can be functionalized to display small peptides to drive cell-targeting delivery of therapeutic nucleotides (18). Limited distribution of pathological vascular remodeling at predictable vascular sites underscores that endothelial inflammation is an attractive target for vascular wall-based therapies. For example, disturbed flow markedly up-regulates vascular cell adhesion molecule 1 (VCAM-1) whose level is high in inflamed endothelium but remains low in healthy endothelium (19–21). We have previously engineered polyelectrolyte complex micelles that display a targeting peptide (VHPKQHR) against VCAM-1 and encapsulate miRNA inhibitors in the core (18). The effectiveness of this targeting polyelectrolyte complex micelle in treating atherosclerosis and vascular complications in vivo has not been tested.

By engineering a new atherogenic mouse line in which miR-92a is selectively induced in adult vascular endothelium, our data demonstrated the causative action of endothelial miR-92a up-regulation and atherosclerosis in vivo, highlighting that endothelial miR-92a is an attractive therapeutic target for atherosclerosis treatments. Moreover, self-assembled VCAM-1–targeting polyelectrolyte complex micelles markedly enhance the therapeutic effectiveness of the miR-92a inhibition strategy to treat atherosclerosis and stenosis induced by disturbed flow. These results provide a proof-of-principle that innovative targeted nanomedicine approaches can be devised for vascular wall-based therapies treating vascular disease.

Results

Endothelial-Specific miR-92a Overexpression Causatively Promotes Atherosclerosis In Vivo. To determine the causal role of endothelial miR-92a in atherogenesis in vivo, we generated an *Apoe*$^{-/-}$ mouse line that enables inducible mR-92a overexpression in adult vascular endothelium. We engineered the inducible miR-92a transgenic line (*miR-92a*^{TG}) by inserting the sequence of *mmu-miR-92a* precursor in the ROSA26 locus in C57BL/6 mice (Fig. 1*A*). The CAG promoter-driven miR-92a transgene was cloned after a PGK-neo-4xPA stop cassette (22) and inactive. The miR-92a transgene then can be activated by removing the PGK-neo-4xPA cassette by Cre recombinase-mediated recombination (Fig. 1*B*). To induce endothelial-specific miR-92a overexpression, the *miR-92a*^{TG} line was bred with *Cdh5(PAC)-CreERT2* mice with an inducible Cre recombinase under the control of the vascular endothelial cadherin (Cdh5) promoter (23), generating the endothelial-specific miR-92a transgenic mouse line (*miR-92a*$^{EC\text{-}TG}$) (Fig. 1*A*). We then crossed the *miR-92a*$^{EC\text{-}TG}$ mice with the atherogenic ApoE-deficient (*Apoe*$^{-/-}$) mice to generate the *miR-92a*$^{EC\text{-}TG}$/*Apoe*$^{-/-}$ mice (Fig. 1*A*). Cdh5-driven Cre recombinase was induced in the *miR-92a*$^{EC\text{-}TG}$/*Apoe*$^{-/-}$ mice by 7 consecutive days of intraperitoneal injection of tamoxifen at week 7, followed by 10-wk high-fat diet feeding (Fig. 1*B*). Endothelial miR-92a overexpression was confirmed by real-time PCR demonstrating a 12.9-fold increase of miR-92a in lung endothelial cells isolated from the tamoxifen-treated *miR-92a*$^{EC\text{-}TG}$/*Apoe*$^{-/-}$ mice when compared to tamoxifen-treated *cdh5(PAC)-CreERT2*/*Apoe*$^{-/-}$ mice (Fig. 1*C*). In agreement with this result, we detected a 7.4-fold increase of miR-92a in the endothelium-enriched mouse carotid intima in the tamoxifen-treated *miR-92a*$^{EC\text{-}TG}$/*Apoe*$^{-/-}$ mice when compared to tamoxifen-treated *Cdh5(PAC)-CreERT2*/*Apoe*$^{-/-}$ mice (Fig. 1*D*). Atherosclerotic burdens were quantified in aortic roots. Oil red O staining demonstrated that the lesion size in the aortic root is markedly increased by 1.6-fold in tamoxifen-treated *miR-92a*$^{EC\text{-}TG}$/*Apoe*$^{-/-}$ mice compared to those in the tamoxifen-treated *Cdh5(PAC)-CreERT2*/*Apoe*$^{-/-}$ mice (Fig. 1 *E* and *F*). The plasma cholesterol was not affected by endothelial miR-92a overexpression (Fig. 1*G*). These results demonstrated that endothelial miR-92a up-regulation per se causally promotes atherogenesis in vivo.

VCAM-1–Targeting Polyelectrolyte Complex Micelles Effectively Encapsulate miR-92a Inhibitors. The atherogenic action of endothelial miR-92a (Fig. 1 *E* and *F*) and its up-regulation by disturbed flow and oxidized low-density lipoprotein (10, 12–14) suggest that miR-92a inhibition in inflamed endothelium is an attractive strategy to lessen atherosclerotic burdens. Induction of endogenous endothelial miR-92a by atherogenic stimuli in these well-established atherosclerosis mouse models (13, 14) suggested that *Ldlr*$^{-/-}$ and *Apoe*$^{-/-}$ mice are ideal models to test the therapeutic effectiveness of the anti–miR-92a therapy. We have previously engineered functionalized polyelectrolyte complex micelles, which display targeting peptides against VCAM-1 expressed in inflamed endothelium, and which simultaneously encapsulate miR-92a inhibitors in the core (18) (Fig. 2*A*). We have further characterized this targeted nanoparticle and its self-assembling process. Briefly, poly-L-lysine (K30) was conjugated to the tail of polyethylene glycol (PEG, molecular weight 2,000) to form a maleimide-terminated bio-macromolecular copolymer. A cysteine-modified VCAM-1–targeting peptide VHPKQHR (24) was grafted on the head of PEG via thiol-maleimide reaction to form three-block polymers (VHPKQHR-PEG-K30). The synthesis steps of VHPKQHR-PEG-K30 polymers are described in *SI Appendix*, Fig. S1.

NMR spectroscopy was used to verify the synthesis of VHPKQHR-PEG-K30 polymers (*SI Appendix*, Fig. S2). Poly-L-lysine is biodegradable and biocompatible; its positive charge effectively complexes negatively charged nucleotides (25). PEG has been shown to enhance the half-time of nanomaterials in circulation (26). VHPKQHR facilitates active binding and intracellular internalization of nanomaterials in inflamed endothelium in vitro and in vivo (24, 27). To determine the condition by which the VHPKQHR-PEG-K30 polymers completely condense miR-92a inhibitor, we conducted an agarose gel retardation assay showing that a mass ratio (polymer/miR-92a inhibitor) of 2 or above resulted in complete miR-92 inhibitor encapsulation with no miR-92a inhibitor leaching (Fig. 2*B*). We further conducted a RiboGreen (RNA detection) assay showing that the encapsulation efficiency of miR-92a inhibitor by the VHPKQHR-PEG-K30 polymers is 92.9% at the mass ration of 2 (polymer/miR-92a inhibitor). Ethidium bromide (EthBr) competitive binding assay further demonstrated the miR-92a inhibitor encapsulation by the VHPKQHR-PEG-K30 polymers (Fig. 2*C*). Specifically, EthBr-stained miRNA inhibitors in the naked form exhibited a strong fluorescence, which was largely abolished when miR-92a inhibitor was first mixed with the VHPKQHR-PEG-K30 polymers (Fig. 2*C*). No significant fluorescence was detected in EthBr in aqueous solution alone (Fig. 2*C*). The ζ-potential of the VHPKQHR-PEG-K30 polymer was 28.5 mV and reduced to 6.5 mV after the electrostatic complexation with the miR-92a inhibitors (Fig. 2*D*).

We performed isothermal titration calorimetry (ITC) to determine the thermodynamic parameters driving the electrostatically dependent, self-assembly process of the targeted polyelectrolyte complex micelle, showing that it is an exothermic reaction with a decrease of enthalpy ($\Delta H = -255.2 \pm 4.9$ kcal/mol) (Fig. 2*E*),

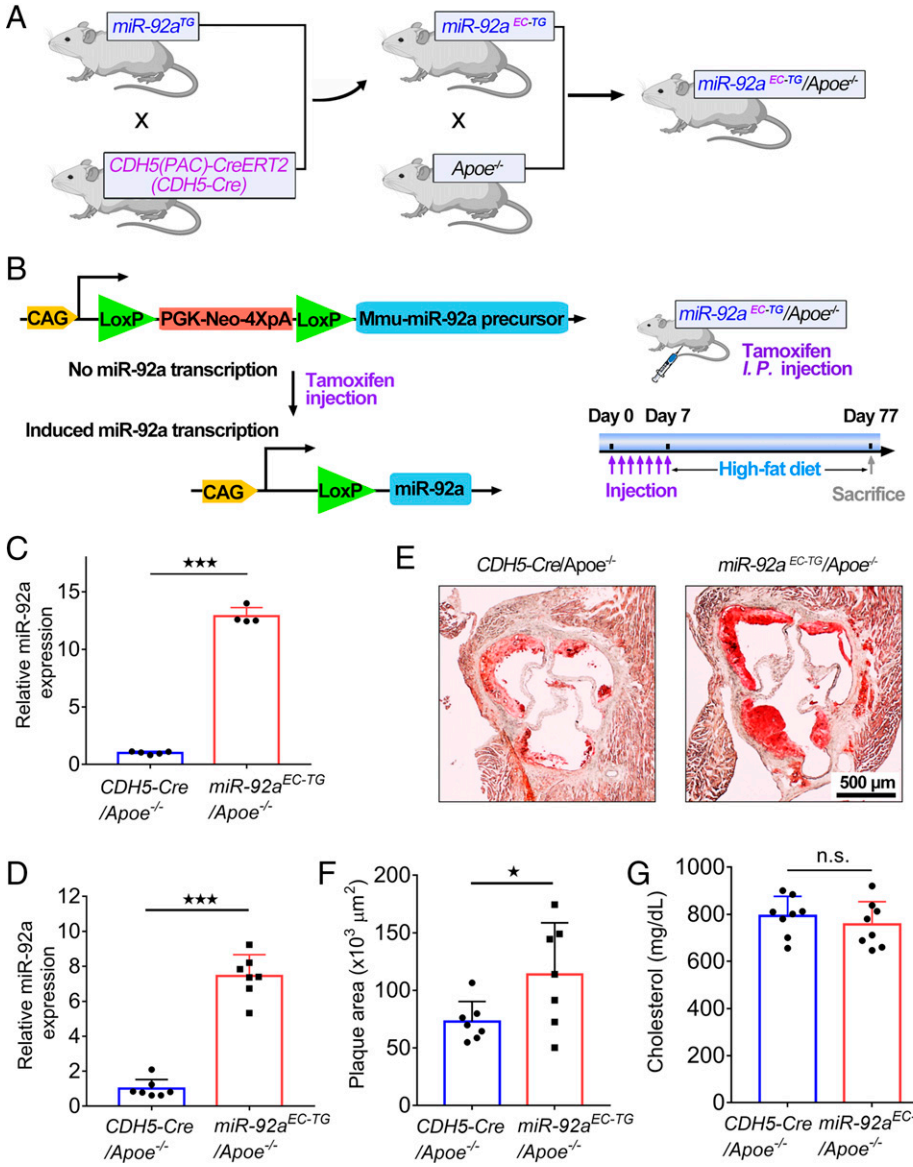

Fig. 1. Increased atherosclerosis in *Apoe*$^{-/-}$ mice by endothelial-specific overexpression of miR-92a. (*A*) Construction of *miR-92a*$^{EC\text{-}TG}$/*Apoe*$^{-/-}$ mice in which miR-92a expression is induced in adult vascular endothelium by tamoxifen injections. The triple transgenic mice (*miR-92a*$^{EC\text{-}TG}$/*Apoe*$^{-/-}$) were engineered by crossing *Apoe*$^{-/-}$ mice with *miR-92a*$^{EC\text{-}TG}$ mice. The *miR-92a*$^{EC\text{-}TG}$ line was generated by breeding the inducible miR-92a transgenic line (*miR-92a*^{TG}) with the *Cdh5*(*PAC*)-*CreERT2* mice with an inducible Cre recombinase under the control of the vascular endothelial cadherin (Cdh5) promoter. The *miR-92a*^{TG} line was generated by inserting the sequence of *mmu-miR-92a* precursor in the ROSA26 locus in the C57BL/6 mice. (*B*) Induction of miR-92a in adult vascular endothelial cells by tamoxifen injections. (*C*) Increased miR-92a expression in lung endothelial cells isolated from tamoxifen-injected *miR-92a*$^{EC\text{-}TG}$/*Apoe*$^{-/-}$ mice compared to lung endothelial cells isolated from tamoxifen-injected *Cdh5(PAC)-CreERT2*/*Apoe*$^{-/-}$ (*CDH5-Cre*/*Apoe*$^{-/-}$) mice (n = 4 to 5 biological samples). (*D*) Increased miR-92a expression in the endothelium-enriched intima of carotid artery in tamoxifen-injected *miR-92a*$^{EC\text{-}TG}$/*Apoe*$^{-/-}$ mice compared to tamoxifen-injected *CDH5-Cre*/*Apoe*$^{-/-}$ mice (n = 7 biological samples). (*E* and *F*) Increased atherosclerosis in the aortic root in tamoxifen-injected *miR-92a*$^{EC\text{-}TG}$/*Apoe*$^{-/-}$ mice compared to tamoxifen-injected *CDH5-Cre*/*Apoe*$^{-/-}$ mice (n = 7 biological samples). (*G*) The plasma cholesterol was not significantly affected by endothelial miR-92a overexpression in tamoxifen-injected *miR-92a*$^{EC\text{-}TG}$/*Apoe*$^{-/-}$ mice compared to tamoxifen-injected *CDH5-Cre*/*Apoe*$^{-/-}$ mice (n = 8 biological samples). Statistical significance was determined by multiple unpaired one-tailed t tests. All error bars are means ± SD. n.s., not significant. *$P \leq 0.05$; ***$P \leq 0.001$.

consistent with the Gibbs free energy (ΔG) of the binding value of −16.54 kcal/mol (Table 1). Micelle self-assembly is associated with a negative change of entropy (ΔS = −0.8 kcal/mol/deg), in agreement with the negatively stained transmission electron microscopy (TEM) images showing monodisperse micelles with a diameter of ∼30.5 nm (Fig. 2*F*) and a median hydrodynamic diameter of 28.2 nm in deionized water (Fig. 2*G*). The abovementioned results collectively demonstrate that the electrostatic interaction drives the exothermic self-assembly process to form electrostatically stable monodisperse nanoparticles composed of the VHPKQHR-PEG-K30 polymers and miRNA inhibitor.

To examine stability further, we conducted dynamic light scattering showing that the micelle size remains relatively constant within a day at room temperature in a few ion-containing physiological buffers, such as phosphate-buffered saline (PBS), PBS containing 10% fetal bovine serum, and endothelial cell culture medium EGM-2 containing 2% fetal bovine serum

Table 1. Thermodynamic parameters of the formation of VCAM-1–targeting polyelectrolyte complex micelles encapsulating miR-92a inhibitor

VCAM-1–targeting micelle

Temperature (°C)	ΔH (kcal/mol)	ΔS (kcal/mol/deg)	ΔG (kcal/mol)
25.17	−255.2 ± 4.9	−0.8	−16.54

(*SI Appendix*, Fig. S3), consistent with previous data showing some storage stability of polylysine-based micelles in physiological solution in vitro (28).

VCAM-1–Targeting Polyelectrolyte Complex Micelles Effectively Deliver miRNA Inhibitors to Inflamed Endothelial Cells In Vitro. We determined the efficacy of VCAM-1–targeting micelles to deliver miRNA inhibitors to inflamed endothelium in vitro. Dye 547–labeled miRNA inhibitors Ctrl were employed to visualize the cellular uptake. Lipopolysaccharides (LPS) were used to induce inflammation in human aortic endothelial cells (HAEC), resulting in markedly increased expression of inflammatory and adhesive molecules, such as E-selectin, CCL2, interleukin (IL)-6, and VCAM-1 (Fig. 3*A*). Control or LPS-treated HAEC were incubated with Dye 547–labeled miRNA inhibitor Ctrl (8 μg/mL), delivered by nontargeting or VCAM-1–targeting micelles, for 30 min. Very limited uptake of Dye 547–labeled miRNA inhibitor Ctrl, delivered by the nontargeting micelles, was detected by confocal microscopy in control HAECs and in LPS-stimulated cells (Fig. 3 *B* and *C*).

In contrast, we detected a significant uptake of Dye 547–labeled miRNA inhibitor Ctrl when delivered by VCAM-1–targeting micelles in LPS-treated HAEC but not in quiescent cells (Fig. 3 *B* and *C*). Flow cytometry analyses verified a significantly increased Dye 547 signal in LPS-stimulated HAEC treated with Dye 547–labeled miRNA inhibitor Ctrl delivered by the VCAM-1–targeting micelles compared to those delivered by nontargeting nanoparticles (Fig. 3*D*), further supporting an enhanced micelle uptake by the VCAM-1–targeting peptide. Pretreatment of LPS-stimulated HAEC with excess free VCAM-1–targeting peptides, which blocked the interaction between the endothelial VCAM-1 and VHPKQHR-displayed micelles, significantly reduced the uptake of Dye 547–labeled miRNA inhibitor Ctrl delivered by the VCAM-1–targeting micelles (Fig. 3*E*). Together, these data demonstrate that VCAM-1–targeting polyelectrolyte complex micelles effectively deliver miRNA inhibitors to inflamed endothelial cells in vitro.

VCAM-1–Targeting Polyelectrolyte Complex Micelles Effectively Deliver miRNA Inhibitors to Inflamed Endothelium In Vivo. We have conducted animal studies showing VCAM-1–targeting micelles effectively deliver miRNA inhibitor to inflamed endothelial cells activated by disturbed flow in vivo, as described in this section. Partial carotid artery ligation was conducted in mice to induce acute disturbed flow in the left carotid artery (LCA) (Fig. 4*A*), which significantly induced VCAM-1 expression in the endothelium (29). Twenty-four hours after the partial carotid ligations, Dye 547–labeled miRNA inhibitor Ctrl (4 mg/kg body weight) were administered to mice via tail veins in the naked form or in complex with nontargeting or VCAM-1–targeting micelles (Fig. 4*B*). Twenty-four hours after the injection, mouse carotids were collected, and *en face* immunofluorescence images were taken to determine the cellular uptake of miRNA inhibitors. Dye 547 signaling is negligible in the $CD31^+$ vascular endothelium in the ligated carotid artery when Dye 547–labeled miRNA inhibitors Ctrl were delivered in the naked form or by nontargeting micelles (Fig. 4 *C* and *D*). In contrast, significant Dye 547 fluorescence was detected in the vascular endothelium in the ligated artery when Dye 547–labeled miRNA inhibitor Ctrl was delivered by VCAM-1–targeting nanoparticles (Fig. 4 *C* and *D*). No significant Dye 547 signal was detected in the quiescent endothelium in the nonligated right carotid artery (RCA) in mice administered with Dye 547–labeled miRNA inhibitor Ctrl in the naked form or in complex with nontargeting or VCAM-1–targeting micelles (Fig. 4*E*). These results collectively demonstrate that VCAM-1–targeting polyelectrolyte complex micelles effectively deliver miRNA inhibitors to inflamed endothelium in vivo.

The Plasma Terminal Half-Life and Biodistribution of Micelles-Delivered miRNA Inhibitor. We determined the pharmacokinetics and biodistribution of the miRNA inhibitor in the naked form or encapsulated in the nontargeting or VCAM-1–targeting micelles. Dye 547–labeled miRNA inhibitor Ctrl (2 mg/kg body weight, naked form or in complex with micelles) was administered to mice via the tail vein. Blood was collected immediately, 30, 60, 120, and 240 min after the injection, followed by fluorescence measurements. *SI Appendix*, Fig. S4 shows that the plasma terminal half-life of Dye 547–labeled miRNA inhibitor Ctrl was not significantly altered by the micelles and the majority of the miRNA inhibitor, whether in the naked form or in complex with the micelles, was cleared in the plasma in an hour. We detected no difference of the half-life of miRNA inhibitor delivered by the VCAM-1–targeting or nontargeting micelles. In a separate mouse experiment, major organs were collected 24 h after the injection of naked or micelle Dye 547–labeled miRNA inhibitor Ctrl. We detected a significant Dye 547 signal in the excised liver and kidney compared to the heart and spleen when miRNA inhibitor was injected in the naked form or encapsulated in the micelles (*SI Appendix*, Fig. S5), providing evidence for clearance through the liver (reticuloendothelial or mononuclear phagocyte system) and the kidney (renal system).

VCAM-1–Targeting, miR-92a Inhibitor-Encapsulated Polyelectrolyte Complex Micelles Significantly Reduced Aortic Atherosclerosis in *Apoe*$^{-/-}$ Mice. The therapeutic effectiveness of the VCAM-1–targeting polyelectrolyte complex in treating vascular complications was tested in vivo. We chose to investigate early-stage atherosclerotic lesions in *Apoe*$^{-/-}$ mice, since previous studies suggested that disturbed flow-induced miR-92a primes vascular endothelium for an enhanced inflammatory response to systemic atherogenic stimuli (10, 13, 14). The study design is illustrated in Fig. 5*A*. *Apoe*$^{-/-}$ mice were fed a high-fat diet starting at 16 wk of age for 4 wk to induce early atherosclerosis. VCAM-1–targeting micelles were loaded with either a miRNA inhibitor control or miR-92a inhibitors (miRIDIAN microRNA Hairpin Inhibitors, Horizon Discovery). These inhibitors are single-stranded (55 nt, hairpins on the ends), chemically enhanced RNA oligonucleotides. Inhibitor control was designed to target *Caenorhabditis elegans* miR-67 (cel-miR-67) and has no effect on human, mouse, and rat miRNAs. Inhibitors against miR-92a are designed to inhibit mature human and mouse miR-92a. One tail-vein injection of PBS, naked miR-92a inhibitor, or VCAM-1–targeting micelles encapsulating miRNA inhibitor controls or miR-92a inhibitors was administered 2 wk after the start of high-fat diet. Inhibitors and inhibitor controls were delivered at 8 mg/kg of body weight. *Apoe*$^{-/-}$ mice were killed at week 20 (after 4 wk of Western diet) for atherosclerosis analysis. Oil red O quantification in aortic roots detected a significant reduction (53%) of atherosclerotic lesions in mice treated with naked miR-92a inhibitors at 8 mg/kg body weight when compared to PBS-treated controls (Fig. 5 *B* and *C*). Notably, aortic root lesion is further decreased when miR-92a inhibitors (8 mg/kg body weight) were administered in the complex with VCAM-1–targeting micelles, by 83% when compared to PBS-treated controls and by 36% when compared to mice administered with naked miR-92a inhibitors (Fig. 5 *B* and *C*). These results demonstrated an

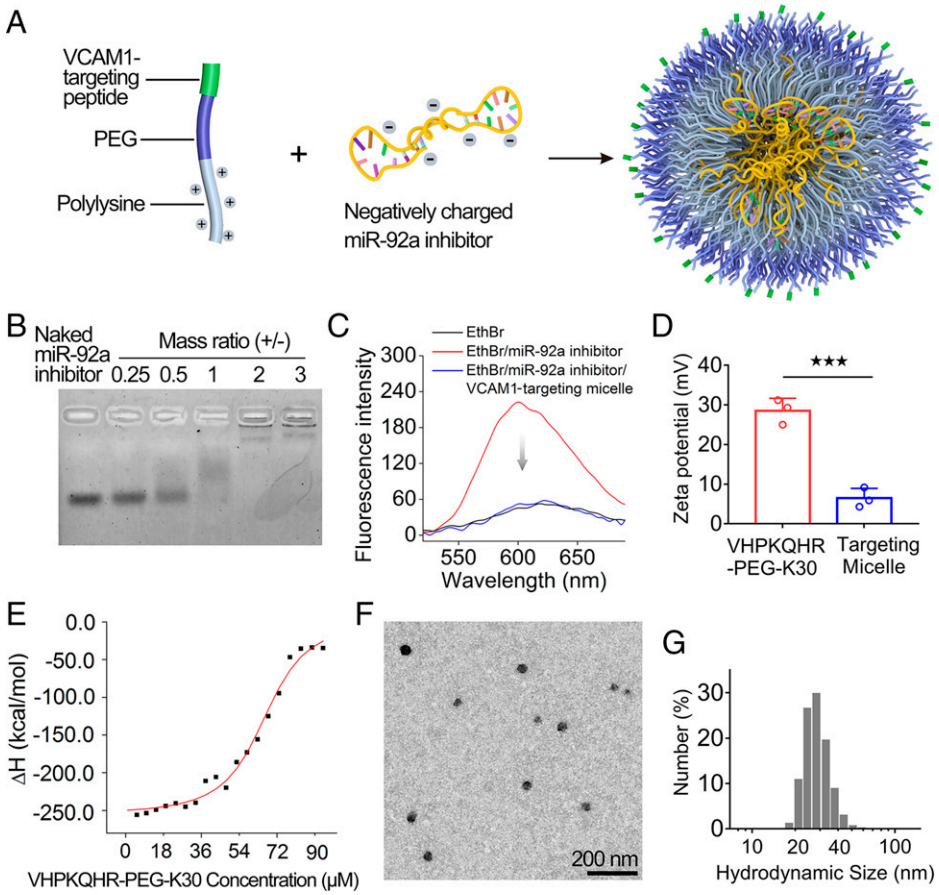

Fig. 2. The formulation and characterizations of VCAM-1–targeting polyelectrolyte complex micelles which encapsulate miRNA inhibitor. (*A*) The illustration of formation of VCAM-1–targeting polyelectrolyte complexes encapsulating miRNA inhibitors in the core. (*B*) Condensation of miRNA inhibitor by the VHPKQHR-PEG-K30 at the mass ratio (polymer/miRNA inhibitor) of 2 or above demonstrated by an agarose gel retardation assay. (*C*) Encapsulation of miRNA inhibitor by the VHPKQHR-PEG-K30 demonstrated by a EthBr competitive binding assay. (*D*) ζ-Potentials of the VHPKQHR-PEG-K30 and VCAM-1–targeting micelles encapsulating miRNA inhibitor ($n = 3$). (*E*) ITC therogram of the assembling of VCAM-1–targeting polyelectrolyte complex micelles encapsulating miRNA inhibitor. (*F*) A negatively stained TEM image of miRNA inhibitor-encapsulated, VCAM-1–targeting polyelectrolyte complex micelles. (*G*) The hydrodynamic diameter of the miRNA inhibitor-encapsulated, VCAM-1–targeting polyelectrolyte complex micelles. Statistical significance was determined by multiple unpaired one-tailed *t* tests. All error bars are means ± SD. ***$P \leq 0.001$.

enhanced therapeutic effectiveness of anti–miR-92a therapy by the VCAM-1–targeting polyelectrolyte complex micelle. Aortic lesions were not affected by administration of VCAM-1–targeting nanoparticles carrying miRNA inhibitor controls, demonstrating that VCAM-1 targeting itself without miR-92a inhibitors has no effect on atherogenesis (Fig. 5 *B* and *C*). Weight (Fig. 5*D*) and plasma cholesterol (Fig. 5*E*) in the *Apoe*$^{-/-}$ mice were not changed by the administration of naked miR-92a inhibitors or targeted nanoparticles. Plasma triglycerides were also not affected by injections of the therapeutic agents (*SI Appendix*, Fig. S6).

We subsequently conducted the experiments using miR-92a inhibitors at 4 mg/kg body weight, hypothesizing that targeted polyelectrolyte complex micelles will enhance the therapeutic effectiveness of miR-92a inhibitors at a lower dose, using the same study design illustrated in Fig. 5*A*. At 4 mg/kg body weight, the naked form of miR-92a inhibitors did not have significant effect on the size of atherosclerotic lesions in the aortic root when compared to those treated with PBS or inhibitor controls (Fig. 5 *F* and *G*). However, we detected a significant reduction of aortic root lesions (by 70% when compared to PBS-treated controls) in *Apoe*$^{-/-}$ mice subjected to one tail-vein injection of miR-92a inhibitors at 4 mg/kg body weight when encapsulated in VCAM-1–targeting polyelectrolyte complex micelles (Fig. 5 *F* and *G*). Lesions were not affected by the injection of VCAM-1–targeting micelles carrying inhibitor controls. Weight (Fig. 5*H*) and plasma cholesterol (Fig. 5*I*) in mice were not changed by the administration of naked miR-92a inhibitors or targeted nanoparticles. These results are consistent with previous studies showing that a high dose (≥16 mg/kg body weight) of naked miR-92a inhibitors conferred antiatherogenic effects and demonstrated that the VCAM-1–targeting polyelectrolyte complex markedly enhances the therapeutic effectiveness of miR-92a inhibition therapies treating atherosclerosis in vivo. Plasma triglycerides were not affected by injections of the therapeutic agents (*SI Appendix*, Fig. S7).

VCAM-1–Targeting, miR-92a Inhibitor-Encapsulated Polyelectrolyte Complex Micelles Markedly Reduce Pathological Vascular Remodeling Induced by Acute Disturbed Flow. We determined the therapeutic potency of the targeted micelles in reducing pathological vascular remolding induced by acute disturbed flow. Partial carotid ligations (Fig. 6*A*) were performed to induce acute disturbed flow in high-fat diet-fed *Apoe*$^{-/-}$ mice, which promotes endothelial inflammation and vascular remodeling. Fourteen days after the ligation, pathological vascular remodeling was shown by Oil red O staining in the ligated LCA, while the RCA developed no sign of vascular remodeling (Fig. 6 *B* and *C*).

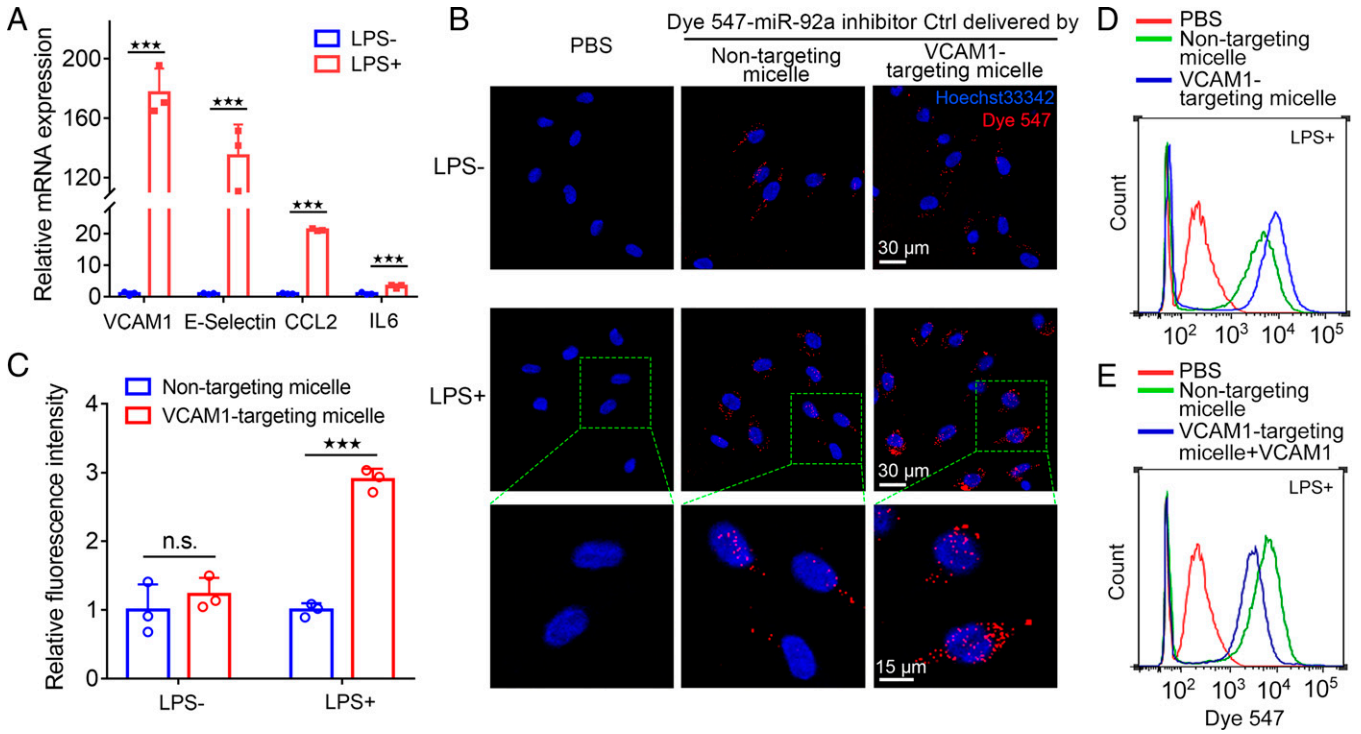

Fig. 3. Delivery of miRNA inhibitor to inflamed cultured vascular endothelial cells by VCAM-1–targeting polyelectrolyte complex micelles in vitro. (*A*) Increased inflammation, demonstrated by elevated expression of VCAM-1, E-Selectin, CCL2, and IL-6 in HAEC treated with LPS ($n = 3$ biological samples). (*B*) Representative confocal images demonstrating the cellular uptake of Dye 547–labeled miRNA inhibitor Ctrl delivered by VCAM1-targeting polyelectrolyte complex micelles in LPS-treated HAEC but not in quiescent control HAEC. Limited cellular uptake of Dye 547–labeled miRNA inhibitor Ctrl, delivered by nontargeting polyelectrolyte complex micelles, in LPS-treated or control HAEC. (*C*) Quantitative analyses of confocal images showing significantly increased cellular uptake of Dye 547–labeled miRNA inhibitor Ctrl delivered by VCAM-1–targeting micelles when compared to nontargeting micelles in LPS-treated HAEC but not in quiescent control HAEC. (*D*) Increased cellular uptake of Dye 547–labeled miRNA inhibitor Ctrl, detected by flow cytometry, by VCAM-1–targeting polyelectrolyte complex micelles compared to nontargeting micelles in LPS-treated HAEC. (*E*) Reduced cellular uptake of Dye 547–labeled miRNA inhibitor Ctrl delivered by VCAM-1–targeting micelles in LPS-stimulated HAEC resulting from the pretreatment with excess free VCAM-1–targeting peptides. Statistical significance was determined by multiple unpaired one-tailed *t* tests. All error bars are means ± SD. n.s., not significant. $***P \leq 0.001$.

Administration of miR-92a inhibitors was at 2 mg/kg, in the naked form or in complexes with VCAM-1–targeting micelles, via the tail vein on days 5, 8, and 11 after the surgery (Fig. 6*A*). Histological sections of liver, kidney, lung, and spleen did not detect significant differences in these tissues in mice subjected to injections of miR-92a inhibitor and targeted micelles when compared to those in PBS-treated controls (*SI Appendix*, Fig. S8). Disturbed flow-induced carotid lesions were markedly reduced (by 89.2%) by the treatment of miR-92a inhibitors delivered by VCAM-1–targeting micelles when compared to PBS-injected controls (Fig. 6 *B–D*). In sharp contrast, injections of naked miR-92a inhibitors at the same regimen had no effect on the carotid lesions induced by acute disturbed flow (Fig. 6 *B–D*). Lesion size was not affected by the injections of VCAM-1–targeting micelles in complex with inhibitor controls (Fig. 6 *B–D*). Serum cholesterol levels (Fig. 6*E*) and body weights (Fig. 6*F*) were not altered by the injections of miRNA inhibitors or nanoparticles. These data again strongly support the enhanced therapeutic effectiveness of anti–miR-92a therapy treating pathological vascular remodeling by the VCAM-1–targeting polyelectrolyte complex micelles.

Discussion

Pathological vascular remodeling, such as occurs in atherosclerosis, stenosis, and surgical interventions, such as arteriovenous fistulas, largely develops at vascular curvatures, bifurcations, and branches where endothelial cells are activated by local disturbed flow (3–5,30). However, current pharmacological therapies of vascular complications mainly target risk factors systemically, but not directly the diseased vasculature per se. The focal nature of atherosclerosis provides a unique opportunity to develop novel therapies targeting disease-causing mechanosensitive mechanisms in endothelium induced by disturbed flow. Previous studies have demonstrated that disturbed flow markedly increases miR-92a expression to promote endothelial dysfunction (10, 12–14), but whether elevated endothelial miR-92a causatively drives atherogenesis in vivo remains to be determined. In addition, targeted delivery of therapeutic nucleotides, such as miR-92a inhibitors to activated endothelium in vivo, remains extremely challenging, limiting future translational developments. In this work, we engineered a mouse line demonstrating that miR-92a overexpression solely in adult vascular endothelium causatively increases atherosclerosis. Moreover, we devised a precision nanomedicine approach targeting inflamed endothelium employing VCAM-1–targeting polyelectrolyte complex micelles, which markedly enhanced the therapeutic effectiveness of the anti–miR-92a therapy in treating atherosclerosis and stenosis in *Apoe*$^{-/-}$ mice. Our results show that dysregulated miRNAs are attractive therapeutic candidates to treat vascular diseases. Moreover, we demonstrated that self-assembled, multifunctional polyelectrolyte complex micelles are an effective nanomedicine strategy to deliver therapeutic nucleotides treating vascular complications in vivo (Fig. 7).

Blood vessels cover 43,000- to 75,000-ft^2 surface areas in an adult human, while vascular disease typically occurs in a very small fraction of this area that is characterized by local inflammation (3–5,30). Antiinflammatory therapy, such as Canakinumab,

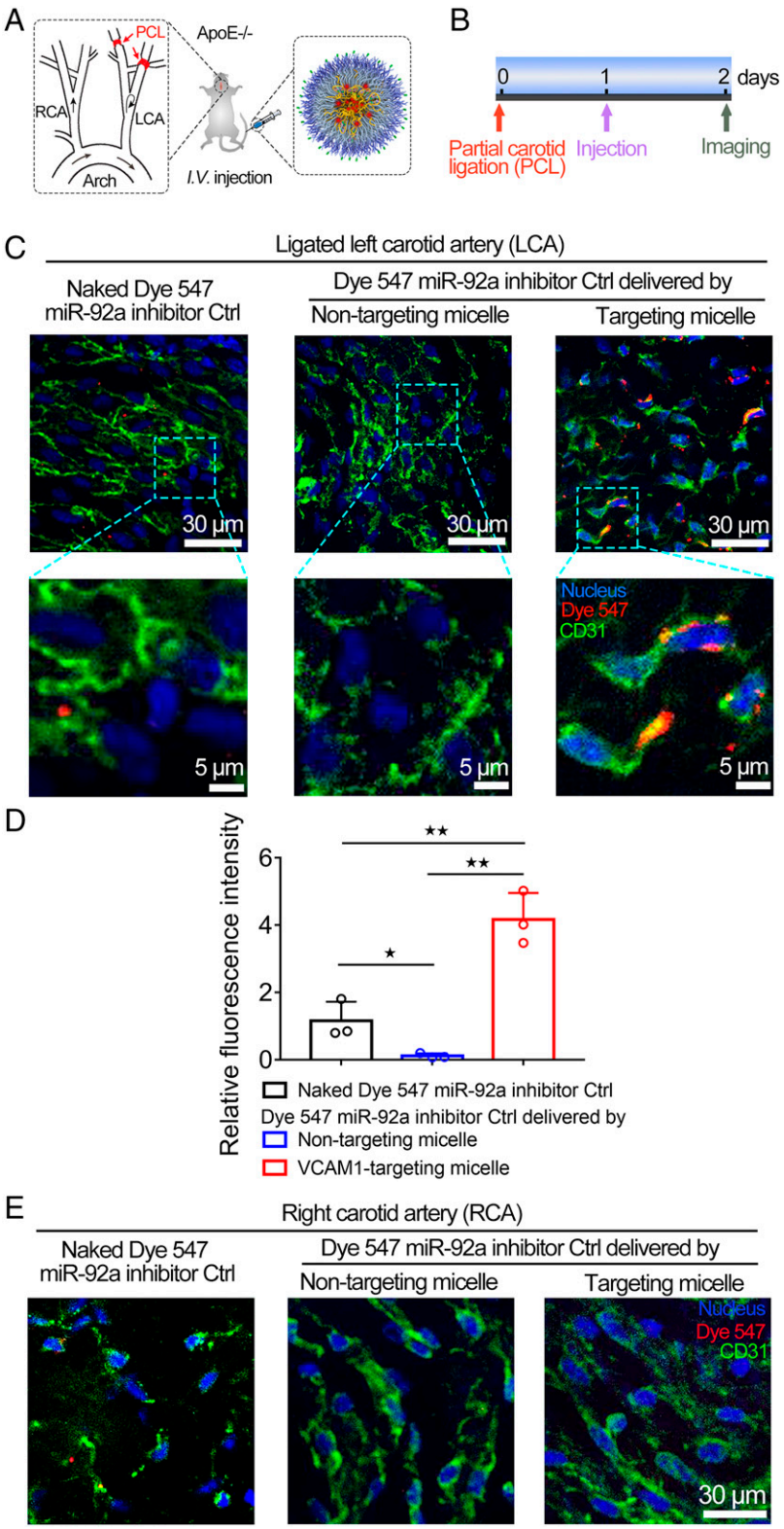

Fig. 4. Delivery of miRNA inhibitors to activated vascular endothelium by VCAM-1–targeting polyelectrolyte complex micelles in vivo. (*A*) A diagram depicting the partial carotid ligation in the LCA in *Apoe*$^{-/-}$ mice and tail-vein injections of Dye 547–labeled miRNA inhibitor Ctrl in the naked form or encapsulated in the polyelectrolyte complex micelles. (*B*) The experimental design. (*C*) *En face* images of ligated left carotid arteries in *Apoe*$^{-/-}$ mice subjected to an injection of Dye 547–labeled miRNA inhibitors Ctrl in the naked form or encapsulated in micelles. Green: CD31; blue: nuclei; red: Dye 547. (*D*) Quantitative analyses of *en face* images showing significantly increased endothelial uptake of Dye 547–labeled miRNA inhibitor Ctrl delivered by VCAM-1–targeting micelles when compared to nontargeting micelles or the naked form of miRNA inhibitor in the ligated mouse carotid artery. (*E*) *En face* images of nonligated right carotid arteries (RCA) in *Apoe*$^{-/-}$ mice subjected to an injection of Dye 547–labeled miRNA inhibitor Ctrl in the naked form or encapsulated in micelles. Green: CD31; blue: nuclei; red: Dye 547. All error bars are means ± SD. *$P \leq 0.05$; **$P \leq 0.01$.

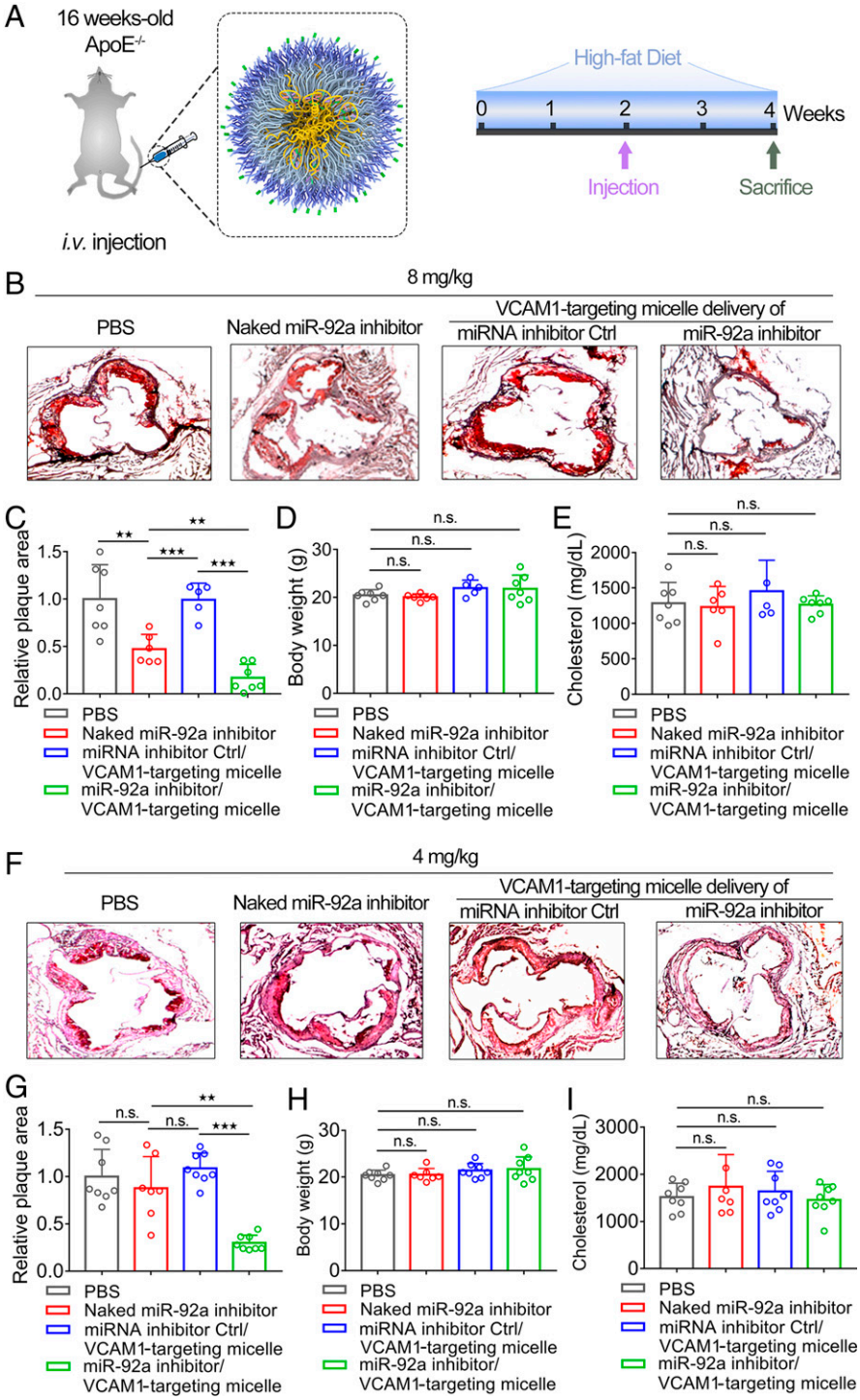

Fig. 5. Enhanced therapeutic effectiveness of the anti–miR-92a therapy treating atherosclerosis in *Apoe*$^{-/-}$ mice by VCAM-1–targeting polyelectrolyte complex micelles. (*A*) The experimental design. (*B*) Representative images of aortic root lesions in *Apoe*$^{-/-}$ mice subjected to an injection of miR-92a inhibitor (8 mg/kg body weight) in the naked form or encapsulated in VCAM-1–targeting micelle or miRNA inhibitor control delivered by VCAM-1–targeting micelles. (*C*) Aortic root lesion quantifications in *Apoe*$^{-/-}$ mice subjected to an injection of miR-92a inhibitor (8 mg/kg body weight) in the naked form or encapsulated in VCAM-1–targeting micelles or miRNA inhibitor control delivered by VCAM-1–targeting micelles (n = 5 to 7 biological samples). (*D*) Body weights and (*E*) cholesterol levels of *Apoe*$^{-/-}$ mice subjected to an injection of miR-92a inhibitor (8 mg/kg body weight) in the naked form or encapsulated in VCAM-1–targeting micelles or miRNA inhibitor control delivered by VCAM-1–targeting micelles (n = 5 to 7 biological samples). (*F*) Representative images of aortic root lesions in *Apoe*$^{-/-}$ mice subjected to an injection of miR-92a inhibitor (4 mg/kg body weight) in the naked form or encapsulated in VCAM-1–targeting micelles or miRNA inhibitor control delivered by VCAM-1–targeting micelles. (*G*) Aortic root lesion quantifications in *Apoe*$^{-/-}$ mice subjected to an injection of miR-92a inhibitor (4 mg/kg body weight) in the naked form or encapsulated in VCAM-1–targeting micelles or miRNA inhibitor control delivered by VCAM-1–targeting micelles) (n = 7 to 8 biological samples). (*H*) Body weights and (*I*) cholesterol levels of *Apoe*$^{-/-}$ mice subjected to an injection of miR-92a inhibitor (4 mg/kg body weight) in the naked form or encapsulated in VCAM-1–targeting micelles or miRNA inhibitor control delivered by VCAM1-targeting micelles (n = 7 to 8 biological samples). Statistical significance was determined by multiple unpaired one-tailed t tests. All error bars are means ± SD. n.s., not significant. $^{**}P \leq 0.01$; $^{***}P \leq 0.001$.

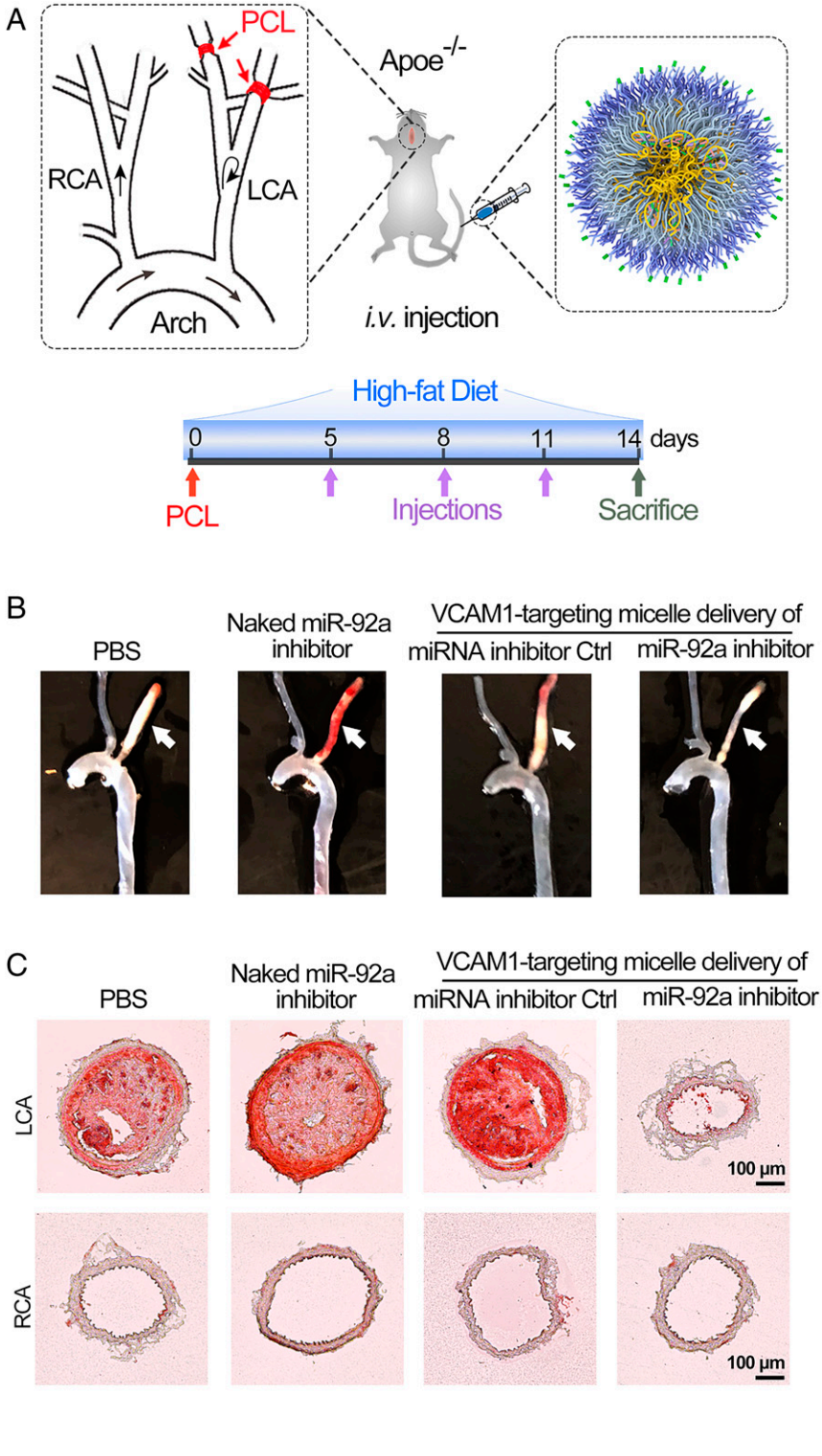

Fig. 6. Enhanced therapeutic effectiveness of the anti–miR-92 therapy treating disturbed flow-induced vascular remodeling in *Apoe*$^{-/-}$ mice by VCAM-1–targeting polyelectrolyte complex micelles. (*A*) The experimental design. (*B*) Representative images of disturbed flow-induced vascular remodeling in the ligated LCA in *Apoe*$^{-/-}$ mice subjected to injections of miR-92a inhibitor (three injections of 2 mg/kg body weight) in the naked form or encapsulated in VCAM-1–targeting micelles or miRNA inhibitor control delivered by VCAM-1–targeting micelles. (*C*) Representative cryosection images of the ligated LCA and nonligated RCA in *Apoe*$^{-/-}$ mice subjected to injections of miR-92a inhibitor (three injections of 2 mg/kg body weight) in the naked form or encapsulated in VCAM-1–targeting micelles or miRNA inhibitor control delivered by VCAM-1–targeting micelles. (*D*) Lesion quantifications of the ligated LCA in *Apoe*$^{-/-}$ mice subjected to injections of miR-92a inhibitor (three injections of 2 mg/kg body weight) in the naked form or encapsulated in VCAM1-targeting micelles or miRNA inhibitor control delivered by VCAM-1–targeting micelles ($n = 6$ biological samples). (*E*) Serum cholesterol levels and (*F*) body weights of *Apoe*$^{-/-}$ mice subjected to injections of miR-92a inhibitor (three injections of 2 mg/kg body weight) in the naked form or encapsulated in VCAM-1–targeting micelles or miRNA inhibitor control delivered by VCAM-1–targeting micelles ($n = 6$ biological samples). Statistical significance was determined by multiple unpaired one-tailed *t* tests. All error bars are means ± SD. n.s., not significant. ***$P \leq 0.001$.

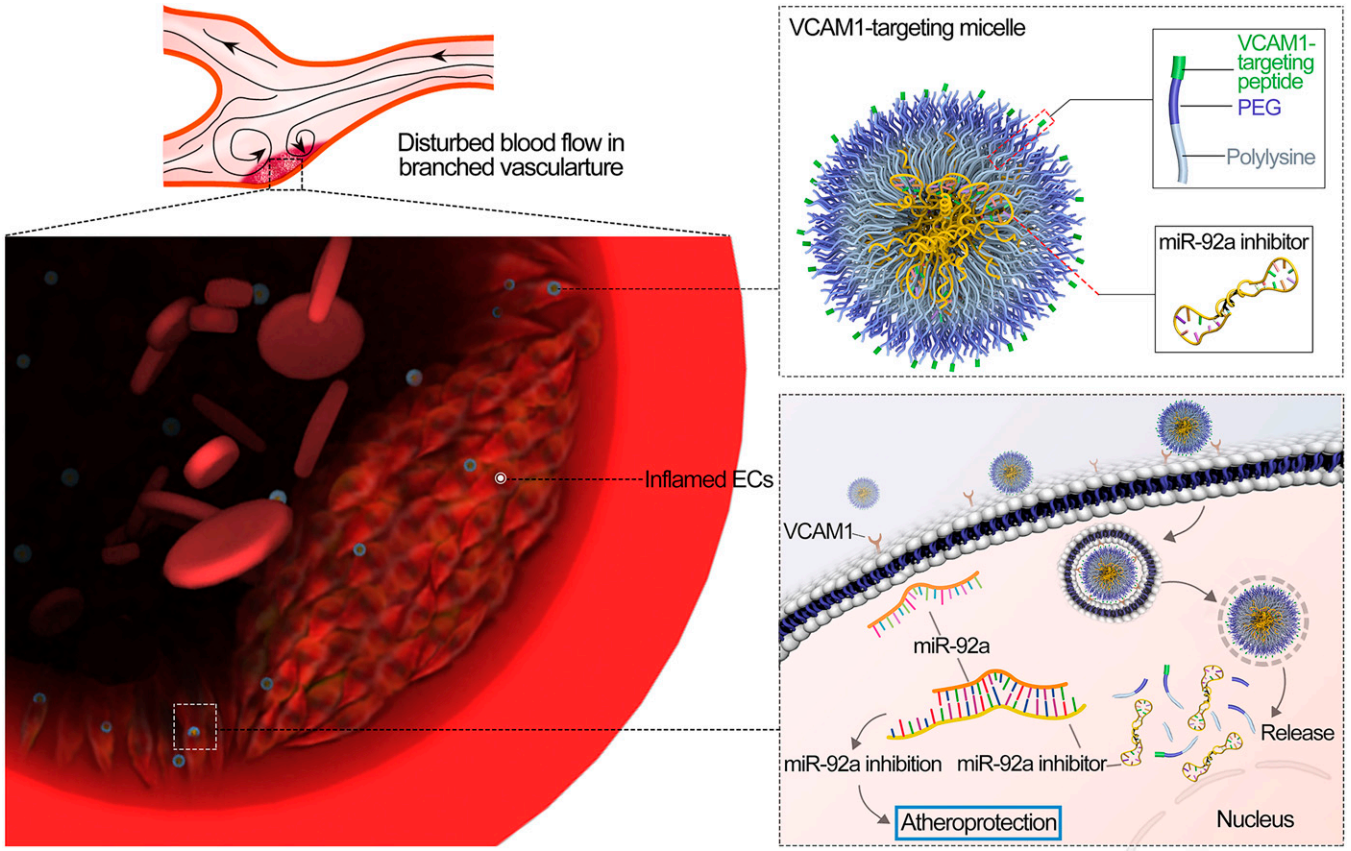

Fig. 7. Schematic diagram depicting that VCAM-1–targeting polyelectrolyte complex micelles deliver miR-92a inhibitor to inflamed endothelial cells treating pathological vascular remodeling induced by local disturbed blood flow.

which inhibits IL-1β, provides unequivocal evidence that atherosclerosis can be treated by suppression of inflammation (31). Nevertheless, controlled vascular inflammation is important for tissue homeostasis and host defense against the pathological organisms. Systemic approaches to reduce vascular inflammation carry the inevitable risk of increased pathogen infections and delaying tissue repair. Indeed, a higher incidence of serious and sometimes fatal infections has been reported in patients treated with canakinumab (31). Previous studies have suggested that nanoscale systems can be engineered to detect the physical, morphological, and cellular attributes of vascular diseases (24, 32–34). This study highlights that nanomedicine, by which innovative nanocarriers are engineered to spatially target inflamed vascular cells, is an attractive strategy to manage local vascular inflammation.

Polyelectrolyte complex micelles are excellent gene-delivery vehicles attributable to their ability to encapsulate charged nucleotides, forming a core by neutralizing the charges via self-assembling, while simultaneously protecting the nucleic acids from nonspecific interactions and enzymatic degradation (16–18). In vivo delivery of therapeutic nucleotides to diseased tissues of interest has often been problematic due to the small size, charge, and instability of the nucleic acid (35). We previously engineered a targeted polyelectrolyte complex micelle that encapsulates miRNA inhibitors in the core and displays targeting peptides against VCAM-1 on the surface (18). In the present work, we further optimized the formulation and characterized this targeted nanoparticle. Agarose gel retardation, EthBr competitive binding assay, ζ-potential measurements, and TEM images collectively demonstrated that miRNA inhibitors were successfully condensed by the VHPKQHR-PEG-K30 polymer, forming nanometer-sized (28 nm) polyelectrolyte complex micelles. ITC measurements demonstrated that this self-assembling process is exothermic with a decrease of enthalpy ($\Delta H = -255.2 \pm 4.9$ kcal/mol), consistent with the ΔG of the binding value of -16.54 kcal/mol. The organization of miRNA inhibitors and PEG-polylysine polymers into a regular micellar structure of consistent size and shape is supported by the TEM images and negative change of entropy ($\Delta S = -0.8$ kcal/mol/deg) after the self-assembling. Supramolecular assembly driven by noncovalent interactions, such as electrostatic interactions here, is valuable for future functional optimization because of its facile modularity; minor changes of individual building blocks may fine-tune the properties of the complex (36–39), a process that might be required to translate this application from mice to humans. Moreover, self-assembly allows the simple preparation by mixing of the components, a clinically approved process successfully employed by recent mRNA vaccines against COVID-19 (40, 41).

Although remaining a tremendously important and prevalent set of health hazards, vascular disease is currently underserved by the nanotechnology community, especially relative to cancer nanomedicine (42–44). To address the ongoing challenges of vascular wall-based therapies targeting diseased blood vessels, we engineered the polyelectrolyte complex micelle to display the VCAM-1–targeting peptide VHPKQHR. Disturbed flow markedly up-regulates VCAM-1 (15), the expression of which increases in activated endothelium but remains low in healthy endothelium (19–21). Our results demonstrate that the VCAM-1–targeting strategy drives active delivery of miRNA inhibitors to inflamed endothelium in vitro and to disturbed flow–activated endothelium in vivo, consistent with previous studies showing that VHPKQHR facilitates VCAM-1–mediated intracellular internalization of nanomaterials in endothelium in vitro and

in vivo (24, 27). VCAM-1 is a major endothelial adhesion molecule mediating inflammation-associated vascular adhesion and leukocyte transendothelial migration. In addition to pathological arterial remodeling, such as atherosclerosis and aneurysm, increased endothelial VCAM-1 is associated with dysfunction of microvasculature such as acute respiratory distress syndrome induced by bacterial or viral (e.g., influenza and SARS-CoV-2 virus) infections (45). A recent study showed that a VCAM-1–targeting antibody significantly enhances the affinity of nanocarriers to inflamed endothelial cells in the cerebral vasculature (46). These results demonstrate a tremendous translational potential of polyelectrolyte complex micelles targeting VCAM-1.

Our transgenic mouse line established the causal action of increased endothelial miR-92a in atherogenesis, further supporting that endothelial miR-92a is an ideal target for atherosclerotic therapies. Reduced atherosclerosis has been reported in *Ldlr*$^{-/-}$ mice and angiotensin II–infused *Apoe*$^{-/-}$/*EC-SREBP2(N)-Tg* mice subjected to systemic administration of miR-92a inhibitors (13, 14). Nevertheless, it is possible that miR-92a inhibition in nonendothelial cells contributes to the reduced atherosclerosis since miR-92a is implicated in cellular homeostasis of various cell types, such as macrophages (47), smooth muscle cells (48), and lymphocytes (49). Our results showed that miR-92a induction solely in adult vascular endothelium causatively promotes atherosclerosis in *Apoe*$^{-/-}$ mice, in agreement with the reduced neointimal hyperplasia in the wire-injured iliac artery in mice with miR-92a deletion in endothelia and leukocytes (50). One limitation of this study is that the therapeutic potency of the VCAM-1–targeting micelles was not tested in the *miR-92a*$^{EC\text{-}TG}$/*Apoe*$^{-/-}$ mice. Another limitation is that we have not determined the therapeutic efficacy of the VCAM-1–targeting, miR-92a inhibitor-encapsulated micelles in promoting advanced lesion regression and treating acute coronary syndromes, which requires future studies in a plaque regression mouse model (51) or large animal studies. Sustained low shear stress resulting from disturbed flow promotes high-risk, rupture-prone plaque by activating local inflammation and matrix degradation (52, 53). Given the critical role of endothelial miR-92a in driving local vascular inflammation induced by disturbed flow (10, 12–15,54), it is plausible that endothelial miR-92a suppression alters the lesion characteristics to promote stable lesions and lessen vulnerable plaques. Moreover, increased miR-92a is associated with reduced endothelial migration and impaired endothelial adhesion to fibronectin (55). Endothelial miR-92a suppression, therefore, may reduce endothelial cell desquamation which leads to superficial erosion and the consequent arterial thrombosis (56).

The future translational potential of miRNA therapies could be limited by high doses of naked miRNA inhibitors/mimics required to achieve therapeutic effectiveness. Employing naked miR-92a inhibitors, reduced atherosclerosis was reported in *Ldlr*$^{-/-}$ mice subjected to six doses at 8 to 16 mg/kg body weight (14) and in *Apoe*$^{-/-}$/*EC-SREBP2(N)-Tg* mice administered with two doses at 16 mg/kg body weight (13). We demonstrated in *Apoe*$^{-/-}$ mice that one injection of naked miR-92a inhibitor at 8 mg/kg body weight, but not at 4 mg/kg body weight, markedly reduced aortic root atherosclerosis. Typically, a high dose and high frequency of administration is required to compensate the rapid degradation of therapeutic nucleotides in the circulation and poor cellular uptake at the targeted sites (7). Our results showed that the antiatherosclerotic action of miR-92a inhibitor at 4 mg/kg body weight can be achieved employing the VCAM-1–targeting polyelectrolyte micelle, consistent with its active targeting capacity to inflamed endothelium. A recent clinical trial reported that single intravenous doses of miR-92a inhibitor (16-bp nucleotides complementary to mature miR-92a developed by miRagen Therapeutics), ranging from 0.01 to 1.5 mg/kg body weight are well tolerated in humans (57).

We tested here the therapeutic effectiveness of miR-92a inhibitor at 2 mg/kg body weight in treating carotid atherosclerosis induced by acute disturbed flow. While three injections of naked miR-92a inhibitor at 2 mg/kg body weight had no effect on the lesion size in the ligated carotid artery, markedly reduced lesions were detected in mice subjected to the same regimen in which miR-92a inhibitor was delivered by VCAM-1– targeting polyelectrolyte complex micelles. These results underscore the significance of targeted delivery strategies for nucleotide-based therapies. Suppression of miR-92a was reported in peripheral blood cells in humans subjected to systemic infusion of miRagen Therapeutic's anti–miR-92a nucleotides (≥0.9 mg/kg) (57). It is possible that the VCAM-1–targeting strategy can reduce the effective therapeutic dosage of miR-92a inhibitor treating vascular inflammation and therefore reduce the off-target side effect of miR-92a suppression in nonendothelial cells, which requires future investigations.

No cellular toxicity has been reported related to polylysine-based nanoparticles (18, 58), suggesting a safety profile that is consistent with our rodent study here showing no significant tissue change in major organs. The safety profile of the polyelectrolyte complex micelles requires further validation in future large animal studies and human clinical trials.

In summary, we elucidated the causal role of elevated endothelial miR-92a in atherogenesis and established the therapeutic effectiveness of VCAM-1–targeting, miR-92a inhibitor-encapsulated polyelectrolyte complex micelles to lessen atherosclerosis and stenosis in vivo. This study established a proof of concept employing innovative nanomedicine approaches to deliver therapeutic nucleic acids treating vascular diseases, the current number one killer in the United States and globally and projected to remain the single leading cause of death for years to come (1). Nucleotide-based therapies have unique potential to revolutionize future medical practice. For example, dysregulated miRNAs can be corrected by specific mimics/inhibitors; disease-causing genes can be silenced by small-interfering RNAs; disease-protective genes can be boosted by transcripts; and genetic mutations can be corrected by genome editing. The unprecedented speed in developing nanotechnology-enabled mRNA-based COVID-19 vaccines has led to exponential advances in nanomanufacturing, large-scale nucleotide synthesis, and cold chain logistics, which are instrumental to the future success of novel nanomedicine therapies (40, 41). The modularity of our polyelectrolyte complex micelle platform allows the capability to present a variety of different cell-targeting mechanisms on the micelle corona and to encapsulate various types of nucleotides in the micelle core. It is our long-term goal to achieve tissue-specific manipulation of multiple disease-causing processes with therapeutic nucleotides since most complex human diseases, such as atherosclerosis and stenosis, are the result of various pathological mechanisms in a wide range of cells and contexts.

Materials and Methods

All studies were conducted in accordance with protocols approved by the Institutional Biosafety Committee or Institutional Animal Care and Use Committee of the University of Chicago. All experimental animals were assigned unique identifiers to blind experimenters to genotypes and treatment. Detailed methods are available in *SI Appendix*.

Data Availability. All study data are included in the article and/or *SI Appendix*.

ACKNOWLEDGMENTS. This work was supported by NIH R01HL138223 and R01HL136765 (to Y.F.), American Heart Association 20TPA35490401 (to Y.F.), and Chicago Biomedical Consortium Accelerator Award A-014 (to Y.F. and M.V.T.).

1. S. S. Virani *et al.*; American Heart Association Council on Epidemiology and Prevention Statistics Committee and Stroke Statistics Subcommittee, Heart disease and stroke statistics-2021 update: A report From the American Heart Association. *Circulation* **143**, e254–e743 (2021).
2. Y. Fang, D. Wu, K. G. Birukov, Mechanosensing and mechanoregulation of endothelial cell functions. *Compr. Physiol.* **9**, 873–904 (2019).
3. J. Zhou, Y. S. Li, S. Chien, Shear stress-initiated signaling and its regulation of endothelial function. *Arterioscler. Thromb. Vasc. Biol.* **34**, 2191–2198 (2014).
4. P. F. Davies, M. Civelek, Y. Fang, I. Fleming, The atherosusceptible endothelium: Endothelial phenotypes in complex haemodynamic shear stress regions in vivo. *Cardiovasc. Res.* **99**, 315–327 (2013).
5. M. A. Gimbrone Jr., G. García-Cardeña, Endothelial cell dysfunction and the pathobiology of atherosclerosis. *Circ. Res.* **118**, 620–636 (2016).
6. C. Hahn, M. A. Schwartz, Mechanotransduction in vascular physiology and atherogenesis. *Nat. Rev. Mol. Cell Biol.* **10**, 53–62 (2009).
7. J. T. Mendell, E. N. Olson, MicroRNAs in stress signaling and human disease. *Cell* **148**, 1172–1187 (2012).
8. E. van Rooij, E. N. Olson, MicroRNA therapeutics for cardiovascular disease: Opportunities and obstacles. *Nat. Rev. Drug Discov.* **11**, 860–872 (2012).
9. C. Urbich, A. Kuehbacher, S. Dimmeler, Role of microRNAs in vascular diseases, inflammation, and angiogenesis. *Cardiovasc. Res.* **79**, 581–588 (2008).
10. Y. Fang, C. Shi, E. Manduchi, M. Civelek, P. F. Davies, MicroRNA-10a regulation of proinflammatory phenotype in athero-susceptible endothelium in vivo and in vitro. *Proc. Natl. Acad. Sci. U.S.A.* **107**, 13450–13455 (2010).
11. Y. Fang, P. F. Davies, Site-specific microRNA-92a regulation of Kruppel-like factors 4 and 2 in atherosusceptible endothelium. *Arterioscler. Thromb. Vasc. Biol.* **32**, 979–987 (2012).
12. K. C. Wang *et al.*, Role of microRNA-23b in flow-regulation of Rb phosphorylation and endothelial cell growth. *Proc. Natl. Acad. Sci. U.S.A.* **107**, 3234–3239 (2010).
13. W. Wu *et al.*, Flow-dependent regulation of Kruppel-like factor 2 is mediated by microRNA-92a. *Circulation* **124**, 633–641 (2011).
14. Z. Chen *et al.*, Oxidative stress activates endothelial innate immunity via sterol regulatory element binding protein 2 (SREBP2) transactivation of microRNA-92a. *Circulation* **131**, 805–814 (2015).
15. X. Loyer *et al.*, Inhibition of microRNA-92a prevents endothelial dysfunction and atherosclerosis in mice. *Circ. Res.* **114**, 434–443 (2014).
16. C. Wu *et al.*, Mechanosensitive PPAP2B regulates endothelial responses to atherorelevant hemodynamic forces. *Circ. Res.* **117**, e41–e53 (2015).
17. A. E. Marras, J. M. Ting, K. C. Stevens, M. V. Tirrell, Advances in the structural design of polyelectrolyte complex micelles. *J. Phys. Chem. B* **125**, 7076–7089 (2021).
18. K. Miyata, N. Nishiyama, K. Kataoka, Rational design of smart supramolecular assemblies for gene delivery: Chemical challenges in the creation of artificial viruses. *Chem. Soc. Rev.* **41**, 2562–2574 (2012).
19. C. H. Kuo *et al.*, Inhibition of atherosclerosis-promoting microRNAs via targeted polyelectrolyte complex micelles. *J. Mater. Chem. B Mater. Biol. Med.* **2**, 8142–8153 (2014).
20. M. J. Davies *et al.*, The expression of the adhesion molecules ICAM-1, VCAM-1, PECAM, and E-selectin in human atherosclerosis. *J. Pathol.* **171**, 223–229 (1993).
21. Y. Nakashima, E. W. Raines, A. S. Plump, J. L. Breslow, R. Ross, Upregulation of VCAM-1 and ICAM-1 at atherosclerosis-prone sites on the endothelium in the ApoE-deficient mouse. *Arterioscler. Thromb. Vasc. Biol.* **18**, 842–851 (1998).
22. M. I. Cybulsky *et al.*, A major role for VCAM-1, but not ICAM-1, in early atherosclerosis. *J. Clin. Invest.* **107**, 1255–1262 (2001).
23. J. Mao, J. Barrow, J. McMahon, J. Vaughan, A. P. McMahon, An ES cell system for rapid, spatial and temporal analysis of gene function in vitro and in vivo. *Nucleic Acids Res.* **33**, e155 (2005).
24. I. Sörensen, R. H. Adams, A. Gossler, DLL1-mediated Notch activation regulates endothelial identity in mouse fetal arteries. *Blood* **113**, 5680–5688 (2009).
25. M. Nahrendorf *et al.*, Noninvasive vascular cell adhesion molecule-1 imaging identifies inflammatory activation of cells in atherosclerosis. *Circulation* **114**, 1504–1511 (2006).
26. C. H. Ahn, S. Y. Chae, Y. H. Bae, S. W. Kim, Synthesis of biodegradable multi-block copolymers of poly(L-lysine) and poly(ethylene glycol) as a non-viral gene carrier. *J. Control. Release* **97**, 567–574 (2004).
27. J. V. Jokerst, T. Lobovkina, R. N. Zare, S. S. Gambhir, Nanoparticle PEGylation for imaging and therapy. *Nanomedicine (Lond.)* **6**, 715–728 (2011).
28. A. Kheirolomoom *et al.*, Multifunctional nanoparticles facilitate molecular targeting and miRNA delivery to inhibit atherosclerosis in ApoE(-/-) mice. *ACS Nano* **9**, 8885–8897 (2015).
29. D. Y. Kwoh *et al.*, Stabilization of poly-L-lysine/DNA polyplexes for in vivo gene delivery to the liver. *Biochim. Biophys. Acta* **1444**, 171–190 (1999).
30. D. Nam *et al.*, Partial carotid ligation is a model of acutely induced disturbed flow, leading to rapid endothelial dysfunction and atherosclerosis. *Am. J. Physiol. Heart Circ. Physiol.* **297**, H1535–H1543 (2009).
31. P. M. Ridker *et al.*; CANTOS Trial Group, Antiinflammatory therapy with canakinumab for atherosclerotic disease. *N. Engl. J. Med.* **377**, 1119–1131 (2017).
32. D. Peters *et al.*, Targeting atherosclerosis by using modular, multifunctional micelles. *Proc. Natl. Acad. Sci. U.S.A.* **106**, 9815–9819 (2009).
33. L. B. Mlinar, E. J. Chung, E. A. Wonder, M. Tirrell, Active targeting of early and mid-stage atherosclerotic plaques using self-assembled peptide amphiphile micelles. *Biomaterials* **35**, 8678–8686 (2014).
34. E. J. Chung *et al.*, Monocyte-targeting supramolecular micellar assemblies: A molecular diagnostic tool for atherosclerosis. *Adv. Healthc. Mater.* **4**, 367–376 (2015).
35. S. Höbel, A. Aigner, Polyethylenimines for siRNA and miRNA delivery in vivo. *Wiley Interdiscip. Rev. Nanomed. Nanobiotechnol.* **5**, 484–501 (2013).
36. R. S. Tu, M. Tirrell, Bottom-up design of biomimetic assemblies. *Adv. Drug Deliv. Rev.* **56**, 1537–1563 (2004).
37. T. Aida, E. W. Meijer, S. I. Stupp, Functional supramolecular polymers. *Science* **335**, 813–817 (2012).
38. H. Acar *et al.*, Self-assembling peptide-based building blocks in medical applications. *Adv. Drug Deliv. Rev.* **110-111**, 65–79 (2017).
39. A. E. Neitzel, Y. N. Fang, B. Yu, A. M. Rumyantsev, J. J. De Pablo, M. V. Tirrell, Polyelectrolyte complex coacervation across a broad range of charge densities. *Macromolecules* **54**, 6878–6890 (2021).
40. S. Friedrichs, D. M. Bowman, COVID-19 may become nanomedicine's finest hour yet. *Nat. Nanotechnol.* **16**, 362–364 (2021).
41. Anonymous, Nanomedicine and the COVID-19 vaccines. *Nat. Nanotechnol.* **15**, 963 (2020).
42. E. J. Chung, M. Tirrell, Recent advances in targeted, self-assembling nanoparticles to address vascular damage due to atherosclerosis. *Adv. Healthc. Mater.* **4**, 2408–2422 (2015).
43. D. R. Lewis, K. Kamisoglu, A. W. York, P. V. Moghe, Polymer-based therapeutics: Nanoassemblies and nanoparticles for management of atherosclerosis. *Wiley Interdiscip. Rev. Nanomed. Nanobiotechnol.* **3**, 400–420 (2011).
44. S. Gadde, K. J. Rayner, Nanomedicine meets microRNA: Current advances in RNA-based nanotherapies for atherosclerosis. *Arterioscler. Thromb. Vasc. Biol.* **36**, e73–e79 (2016).
45. R. T. Huang *et al.*, Experimental lung injury reduces Krüppel-like factor 2 to increase endothelial permeability via regulation of RAPGEF3-Rac1 signaling. *Am. J. Respir. Crit. Care Med.* **195**, 639–651 (2017).
46. O. A. Marcos-Contreras *et al.*, Selective targeting of nanomedicine to inflamed cerebral vasculature to enhance the blood-brain barrier. *Proc. Natl. Acad. Sci. U.S.A.* **117**, 3405–3414 (2020).
47. L. Lai *et al.*, MicroRNA-92a negatively regulates Toll-like receptor (TLR)-triggered inflammatory response in macrophages by targeting MKK4 kinase. *J. Biol. Chem.* **288**, 7956–7967 (2013).
48. L. Zhang *et al.*, miR-92a inhibits vascular smooth muscle cell apoptosis: Role of the MKK4-JNK pathway. *Apoptosis* **19**, 975–983 (2014).
49. C. Xiao *et al.*, Lymphoproliferative disease and autoimmunity in mice with increased miR-17-92 expression in lymphocytes. *Nat. Immunol.* **9**, 405–414 (2008).
50. J. M. Daniel *et al.*, Inhibition of miR-92a improves re-endothelialization and prevents neointima formation following vascular injury. *Cardiovasc. Res.* **103**, 564–572 (2014).
51. B. Hewing *et al.*, Rapid regression of atherosclerosis with MTP inhibitor treatment. *Atherosclerosis* **227**, 125–129 (2013).
52. Y. S. Chatzizisis *et al.*, Prediction of the localization of high-risk coronary atherosclerotic plaques on the basis of low endothelial shear stress: An intravascular ultrasound and histopathology natural history study. *Circulation* **117**, 993–1002 (2008).
53. K. C. Koskinas *et al.*, Natural history of experimental coronary atherosclerosis and vascular remodeling in relation to endothelial shear stress: A serial, in vivo intravascular ultrasound study. *Circulation* **121**, 2092–2101 (2010).
54. M. D. Krause *et al.*, Genetic variant at coronary artery disease and ischemic stroke locus 1p32.2 regulates endothelial responses to hemodynamics. *Proc. Natl. Acad. Sci. U.S.A.* **115**, E11349–E11358 (2018).
55. A. Bonauer *et al.*, MicroRNA-92a controls angiogenesis and functional recovery of ischemic tissues in mice. *Science* **324**, 1710–1713 (2009).
56. P. Libby, G. Pasterkamp, F. Crea, I. K. Jang, Reassessing the mechanisms of acute coronary syndromes. *Circ. Res.* **124**, 150–160 (2019).
57. W. T. Abplanalp *et al.*, Efficiency and target derepression of anti-miR-92a: Results of a first in human study. *Nucleic Acid Ther.* **30**, 335–345 (2020).
58. Z. He, Y. Sun, J. Cao, Y. Duan, Degradation behavior and biosafety studies of the mPEG-PLGA-PLL copolymer. *Phys. Chem. Chem. Phys.* **18**, 11986–11999 (2016).